Distributed RIS-Based Sensing of Mobile Passive Obstacles in Dense mmWave Networks

Tan-Tho LUC, Lélio CHETOT, Francesca COSTANZO, Benoît DENIS
CEA-Leti, Université Grenoble Alpes, F-38000 Grenoble, France
{tan-tho.luc, lelio.chetot, francesca.costanzo, benoit.denis}@cea.fr

***Abstract*—The millimeter-wave (mmWave) technology offers unprecedented potential to meet the growing demand for high-speed data communications. However, it is also highly sensitive to radio obstructions, which can significantly degrade the quality of service and require frequent handover operations. Anticipating such blockages through environment sensing is therefore critical for efficient radio resource management and improved network performance. In this context, this paper proposes an opportunistic and cooperative sensing approach based on spatially distributed dual-beam reflective Reconfigurable Intelligent Surfaces (RISs). These surfaces scan the environment and reflect toward sensing nodes the ambient signal power from a plurality of non-coherent sources. By analyzing the power fluctuations eventually caused by transient shadowing, the presence of a mobile blocker is first detected in angular sectors centered around the RISs. This information can then be shared and fused to position the blocker in 2D. As passive surfaces can suffer from significant power losses and irregular beam patterns leading respectively to false alarms and missed detections, we thus consider selecting and/or weighting the RIS-wise detection observations that feed the final cooperative positioning stage, relying on empirical reliability indicators inspired by image processing. Simulation results in a dense mmWave scenario illustrate benefits from selective multi-RIS cooperation.**

***Index Terms*—Radio blockage prediction, Passive mobile obstacles, mmWave communications, Network densification, 6G networks, Integrated sensing and communications, Reconfigurable intelligent surfaces, Cooperative positioning.**

I. INTRODUCTION

Over the past decade, the millimeter-wave (mmWave) technology, leveraging abundant spectrum between 28–300 GHz, has emerged as a key solution for high-speed, ultra-low latency data transmission. However, radio links are more prone to interruptions when operating at high frequency. The overall network performance is thus degraded due to a reduced quality of service (QoS) experienced by user equipments (UEs), which must trigger frequent handover procedures [1]. Anticipating link blockages through large-scale in-band environment sensing is hence of paramount importance to develop efficient radio resource management and handover mechanisms. In this context, the emerging paradigm of integrated sensing and communication (ISAC) has recently gained significant attention, particularly for future 6G networks.

State-of-the-art approaches consider relatively “late” detection mechanisms, relying on adjacent guard beams alongside the main BS-UE communication beam [2] or on empirical statistics of the direct path received power [3]. In [4], another in-band detection method inspired by device-free localization techniques [5] leverages the transient power shadowing induced by a mobile blocker. Specifically, it tracks temporal fluctuations in ambient interference power from nearby transmitters via side-lobes. A *sensing matrix* formed from measured signal-to-sector interference-plus-noise ratio is processed via a source separation method (e.g., Singular Value Decomposition (SVD)) to recover the mobile blocker’s space-time power profile and its angular sector occupancy. The previous approach has been extended in [6], where the blocker’s position is estimated as the intersection of angular sectors detected from multiple nodes via cooperative sensing using a least squares (LS) approach [7]. In [2], [4], [3], [6] the sensing field of view is geographically restricted to the immediate vicinity of a pre-existing communication link. Moreover, these solutions require a minimal network deployment of active communicating nodes. Finally, sensing nodes with dedicated hardware must be deployed (e.g., sectored antenna systems [4], [6] or multibeam capabilities including guard beams [2]). Even more specific solutions require a side radio technology [8] or the preliminary in-site learning of the radio environment, adding a critical offline calibration phase (e.g., [9], [10]).

In this paper, we consider a plurality of spatially distributed dual-beam reflective Reconfigurable Intelligent Surfaces (RISs), which can be for instance implemented with interconnected uniform phased arrays or transmit-arrays [11], or even with surface-wave metaprisms [12]. Each of these surfaces, which is associated with a standard communicating node (serving also as collecting sensing node), is endowed with at least one programmable "input" beam. The latter scans angular regions of space, therefrom, reflecting towards the sensing node the ambient signal power integrated from non-coherent sources residing in these angular regions. This approach aims at relaxing the constraints in terms of both hardware requirements and scanning protocol in comparison with [4], while still benefiting from spatial diversity and information redundancy thanks to multi-point sensing like in [6]. One drawback of using passive low-complexity RISs is less favorable received power dynamics due to extra path loss between the RIS and its sensing node, increasing missed detections of the blocker. Additionally, wide main lobes (i.e., relatively to the blocker’s size) and irregular beam patterns (e.g., with significant secondary lobes) increase false alarms. To mitigate these effects prior to positioning, we first apply a similarity score to the SVD-based power source separation. This score quantifies how closely the raw

sensing matrix matches the reconstructed structural channel alone (i.e., excluding the presumed blocker's contributions). It enhances SVD-based signal separation and serves as an indicator of the reliability of the blocker's space-time power signature used for the detection of occupied angular sectors. Accordingly, in the cooperative positioning step itself, we consider weighting/selecting observations associated with the different RISs, depending on the distribution of their respective similarity scores (over the sectors). Simulation results in a dense mmWave network scenario illustrate the performance of the proposed solution, as well as limitations inherent to the use of RISs in terms of exploitable signal dynamics.

II. System model

A. Dense RIS-enabled mmWave Network

We consider a 2-dimensional mmWave network with $N \in \mathbb{N}$ UEs served by $M \in \mathbb{N}$ densely deployed BSs. Each UE is associated with its nearest BS. The network contains also J remotely controllable dual-beam reflective RISs, whose positions and absolute orientations are known. The closest UE to a RIS is treated as a *sensing node* (SN) which collects RIS-reflected signals from any signal sources (e.g., other UEs and/or BSs active in transmission). RIS $j \in [\![1, J]\!]$ is able to scan its environment with its *input* beam over a discrete set of azimuth steering angles $\boldsymbol{\psi}_j = [\psi_{j,s}]_{s\in[\![1,S]\!]}$, assuming non-overlaping sensed angular sectors of width α_j (See Fig. 1). All the necessary coarse synchronization, beam training and beam alignment operations are assumed to be performed during an initial access phase, thus focusing only on steady-state sensing. Hence the maximum directivity gains are preliminarily configured for both communication (between all UEs and their serving BSs) and sensing (between sensing nodes and their associated RISs).

Similarly to [4], we consider the presence of a unique *blocker*, i.e. a cylindrical passive object with radius R_B moving in the network with a relatively low velocity (e.g. walking human, industrial or wheeled mobile robots), causing temporary radio blockages. Even though we assume a unique mobile blocker, our approach could be extended to detect multiple blockers too. In particular, one could benefit from the spatial diversity resulting from the multi-RIS sensing, which is therefore left for future works.

We denote by $\mathcal{U} = \{\boldsymbol{u}_n \mid n \in [\![1, N]\!]\}$, $\mathcal{B} = \{\boldsymbol{b}_m \mid m \in [\![1, M]\!]\}$ and $\mathcal{R} = \{\boldsymbol{r}_j \mid j \in [\![1, J]\!]\}$ the subsets of $\mathbb{R}^2$ of UE, BS and RIS positions and by $\boldsymbol{p}_B[k] \in \mathbb{R}^2$ the blocker's position at time k.

B. Received Power Measurements at RIS-aided Sensing Nodes

We assume a simple Friis path-loss model, where the average received power $P_{\mathrm{Rx}}[k]$ over any peer-to-peer transmission link under blocker's shadowing at instant k is given by

$$P_{\mathrm{Rx}}(t) = P_{\mathrm{Tx}} G_{\mathrm{Tx}} G_{\mathrm{Rx}} G_{\mathrm{PL}}(d) \chi[k] \zeta \tag{1}$$

where

- P_{Tx} is the transmit power;
- G_{Tx} and G_{Rx} are the transmitter and receiver antenna gains respectively;
- $G_{\mathrm{PL}}(d)$ is the path-loss gain at distance d;
- $\chi[k] = A\exp(-0.125 R_B^{-2} \psi_B[k]^2)$ is the shadowing coefficient due to the blocker[1], where A represents fully-shadowed attenuation and $\psi_B[k]$ is the relative blocker angle to the radio link [4], [6].
- ζ represents other constant random shadow-fading contributions (i.e., besides the blocker's obstruction), considering that fast-fading fluctuations have been averaged out

For $(j, s) \in [\![1, J]\!] \times [\![1, S]\!]$ at time k, the j-th SN receives power $p_{j,s}[k]$ from its RIS, aggregating reflected signal contributions from $I \in \mathbb{N}$ non-coherent sources[2] while applying the RIS steering angle $\psi_{j,s}$. This power is expressed as

$$p_{j,s}[k] = G_{R,\mathrm{SN}}(d_j, \psi_{j,0}) \sum_{i=0}^{I} G_{\mathrm{in}}(\psi_{j,s}, \psi'_{j,i}) p_{j,i}[k] \tag{2}$$

with

$$G_{R,\mathrm{SN}}(d_j, \psi_{j,0}) = G_0(d_j) G_{\mathrm{out}}(\psi_{j,0}) G_{\mathrm{SN}} \tag{3}$$

where

- d_j is the distance between the SN and the RIS;
- $p_{j,i}[k]$ is the power of the signal from the i-th source impining onto the RIS, calculated with (1);
- $G_{\mathrm{in}}(\psi_{j,s}, \psi'_{j,i})$ is the gain of the RIS input beam pointing at the steering angle $\psi_{j,s}$ with an angle of arrival $\psi'_{j,i}$ w.r.t. source i, both defined relatively to a local reference, chosen here as the normal to the RIS (see Fig 1).
- $G_{\mathrm{out}}(\psi_{j,0})$ is the RIS output beam gain pointing towards the SN in the direction $\psi_{j,0}$;
- $G_0(d_j)$ is the average channel gain between the j-th RIS and SN, including path loss and constant shadow effects;
- G_{SN} is the gain of the SN receive antenna.

III. Proposed Cooperative multi-RIS Sensing Scheme

A. Detection of Occupied Angular Sectors

To detect the angular sectors where the blocker may be present, each SN maintains a *sensing matrix* spanning a window of Δ time steps for each RIS steering angle. Hence, at time index $k \in \mathbb{N}$, the j-th SN collects S power measurements from the sweeping of its RIS input beam over all the addressable steering angles $\boldsymbol{\psi}_j$, as follows

$$\boldsymbol{P}_j[k] = \begin{pmatrix} p_{j,1}[k-\Delta+1] & \dots & p_{j,1}[k] \\ \vdots & \dots & \vdots \\ p_{j,S}[k-\Delta+1] & \dots & p_{j,S}[k] \end{pmatrix}. \tag{4}$$

When the RIS input sensing beam (in the current steering direction) is blinded by the blocker, the power received from surrounding non-coherent sources, lying in the corresponding

[1]We assume static and non blocking BSs and UEs.

[2]Sources "outside" the currently aimed sector s may still contribute to the collected received power through side lobes of the RIS beam pattern.

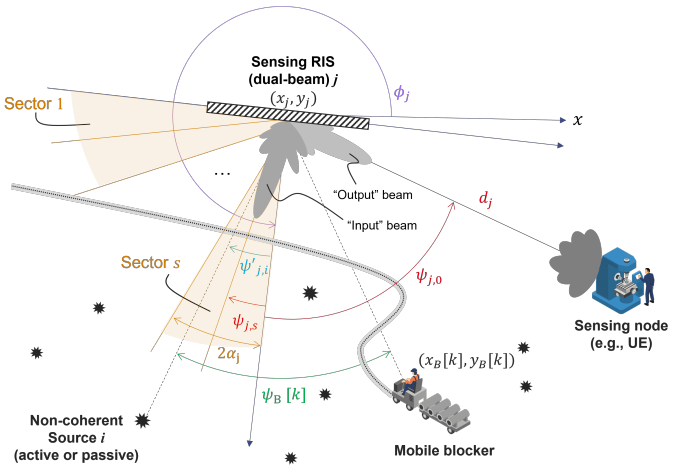

Fig. 1: Sensing principle with a dual-beam RIS reflecting ambient signals from non-coherent sources towards a Rx sensing node, under transient obstructions caused by a mobile obstacle.

angular sector, may experience significant fluctuations between consecutive sensing instants. Hence, the terms under the summation in (2) may vary significantly between each sweeping operation due to blocker's shadowing, while all other dominant contributions are expected to stay constant in first approximation. Accordingly, for each RIS j, the sensing matrix can be viewed as the sum of three main components:

$$\boldsymbol{P}_j[k] = \boldsymbol{C}_j[k] + \boldsymbol{B}_j[k] + \boldsymbol{N}_j[k] \tag{5}$$

where $\boldsymbol{B}_j[k]$ is the blocker's space-time power signature, $\boldsymbol{C}_j[k]$ comprises the structural channel contributions, while $\boldsymbol{N}_j[k]$ captures all other random fluctuations.

Similar to [4], [6], we then apply a blind source separation technique based on SVD, decomposing the sensing matrix into a product of three matrices as follows:

$$\boldsymbol{P}_j[k] = \boldsymbol{U}_j[k]\boldsymbol{\Sigma}_j[k]\boldsymbol{V}_j[k]^T \tag{6}$$

where $\boldsymbol{U}_j[k] \in \mathbb{R}^{S\times r}$, $\boldsymbol{V}_j[k] \in \mathbb{R}^{\Delta\times r}$, and $\boldsymbol{\Sigma}_j[k] \in \mathbb{R}^{r\times r} = \mathrm{diag}(\sigma_1, \sigma_2, \ldots, \sigma_r)$ with $r = \mathrm{rank}(\boldsymbol{P}_j[k]) \leq \min(S, \Delta)$ and $\sigma_1 \geq \cdots \geq \sigma_r > 0$ are the singular values and

$$\boldsymbol{P}_j[k] = \underbrace{\sum_{l=1}^{l_0} \sigma_l \mathbf{u}_{j,l}\mathbf{v}_{j,l}^T}_{\boldsymbol{C}_j[k]} + \underbrace{\sum_{l=l_0+1}^{l_1} \sigma_l \mathbf{u}_{j,l}\mathbf{v}_{j,l}^T}_{\boldsymbol{B}_j[k]} + \underbrace{\sum_{l=l_1+1}^{r} \sigma_l \mathbf{u}_{j,l}\mathbf{v}_{j,l}^T}_{\boldsymbol{N}_j[k]}, \tag{7}$$

where $\mathbf{u}_l$ (resp. $\mathbf{v}_l$) are the columns of the semi-unitary matrix $\boldsymbol{U}_j[k]$ (resp. $\boldsymbol{V}_j[k]$) and $1 \leq l_0 \leq l_1 \leq r$.

An adequate selection of l_0 and l_1 enables to retrieve the blocker's signature matrix $\boldsymbol{B}_j[k]$. Although they can be chosen by finding abrupt changes in the singular values [4], [6], here, we propose an adaptive selection scheme based on a similarity metrics between $\boldsymbol{P}_j[k]$ and $\boldsymbol{C}_j[k]$, e.g. using the similarity index measure (SSIM) inspired by image processing [13]. Assuming $\boldsymbol{N}_j[k]$ is negligible against $\boldsymbol{C}_j[k]$ and $\boldsymbol{B}_j[k]$, a similarity matrix $\boldsymbol{M}_j[k]$ exhibiting high-valued entries means that $\boldsymbol{P}_j[k]$ and $\boldsymbol{C}_j[k]$ are very similar. Hence, only little power fluctuations are left to interpretation in $\boldsymbol{B}_j[k]$ for detection purposes. Interpreting the absolute signal level in $\boldsymbol{B}_j[k]$ to directly assess detection quality has proved very challenging (typically, due to the high variability of the sector-wise received power from ambient sources). This similarity metrics can hence serve as meaningful proxy (See Sec. III-C).

The selection of l_0 is finally performed iteratively starting with an initial guess of 1, and then incrementally increasing its value until the mean similarity $\bar{M}_j[k] = \sum_{s=1}^{S}\sum_{t=1}^{\Delta}[\boldsymbol{M}_j[k]]_{s,t}/(S\Delta) < M^\star$ for some threshold $M^\star$. Then, a decision is made based on the corresponding matrix $\boldsymbol{B}_j[k]$ regarding a possible angular sector occupancy, by selecting the sector index $\hat{s}_j[k] = \arg\max_{s\in[\![1,S]\!]}[\boldsymbol{b}_j[k]]_s$.

When such a detection occurs for a particular RIS j at time index k, the *occupied sector* $\hat{s}_j[k]$ is then associated with the corresponding relative steering angle $\hat{\psi}_{\hat{j}}[k]]$. The set of all relative angles over the available RISs is $\hat{\boldsymbol{\psi}}[k] = [\hat{\psi}_j[k]]_{j\in[\![1,J]\!]}$

Both SVD and SSIM are widely used and lightweight implementations are available (e.g., built-in SVD in Matlab and Python [14], or fast SSIM [15]). In addition, the sensing matrix has a relatively small size. The proposed processing framework is hence expected to comply with most real-time embedded applications (typically, running at standard UEs).

B. Cooperative Sector-based Positioning Algorithm

Each SN could individually compute a gross estimate of the blocker position based on their detected occupied sectors. However, such an estimation would be imprecise due to the uncertainty in the detection process and the angular quantization while scanning. Therefore, we assume the RIS scanning operations to be coordinated and SNs to synchronously share angular detection information, either with each other or with a fusion center. Such a cooperative strategy thus contribute to improve the estimated global position of the blocker.

The relative orientations of the detected occupied sectors $\hat{\boldsymbol{\psi}}[k] = [\hat{\psi}_j[k]]_{j\in[\![1,J]\!]}$ are converted into absolute angles $\boldsymbol{\theta}[k] = \boldsymbol{\psi}[k] + \boldsymbol{\phi}$ where $\boldsymbol{\phi} = [\phi_j]_{j\in[\![1,J]\!]}$ denote the RISs' absolute orientations w.r.t. an arbitrary global reference system (e.g., all absolute angles are defined with respect to the $[0, x)$ axis following the usual direct trigonometric convention).

For a RIS $j \in [\![1, J]\!]$ where the blocker has been detected, we consider the tuple $(\boldsymbol{r}_j, \theta_j, \alpha_j)$, where $2\alpha_j$ is the angular width of the occupied sector, which accounts for the RIS input beam width, the azimuth granularity applied in RIS beam scanning, but also on the quality of detection itself.

To compute the intersection of all the detected occupied sectors, we propose an approach based on weighted least squares (WLS) extending the approaches initially proposed in [6], [7]. More specifically, for a given sector with absolute angle θ_j, $\epsilon_j \in [-\alpha'_j[k], \alpha'_j[k]]$ is the relative angular error w.r.t. the sector orientation[3]. Let (x_j^*, y_j^*) define the closest point to $(\hat{x}_B, \hat{y}_B)$ along the line crossing (x_j, y_j) with orientation $\theta_j + \epsilon_j$. The optimization problem thus consists in finding the

[3]In the best case, the assumed uncertainty $\alpha'_j[k] = \alpha_j$.

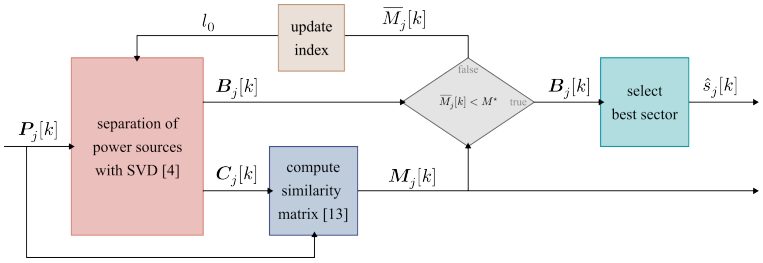

Fig. 2: Sector detection process with adaptive SVD-based power source separation and similarity comparison.

location that minimizes the Euclidean distances between the estimated position of the blocker and the points (x_j^*, y_j^*):

$$(\hat{x}_B, \hat{y}_B) = \underset{(x,y)}{\arg\min} \sum_{r_j \in \mathcal{R}_0} \left((x - \mathbb{E}_{\epsilon_j}[x_j^*])^2 + (y - \mathbb{E}_{\epsilon_j}[y_j^*])^2 \right) \tag{8}$$

The value of $\alpha'_j[k]$ is the relative uncertainty of detected sector of RIS j, which can be empirically calculated according to one of the methods in the following III-C.

Like in [6], after a few mathematical manipulations, one can show that the 2D position of the blocker can be estimated by solving a linear equation. This solution can be efficiently computed at any of the sensing nodes or at a central fusion center indifferently, after gathering information from the co-operative sensing nodes. Complete analytical expressions of this solution can be found in [6].

C. Processing of Detected Angular Sectors before Positioning

The matrix $\boldsymbol{B}_j[k]$ captures not only the desired shadowing effects caused by the moving object but also fluctuations in other sectors, mainly via the RIS side lobes. This may prevent from extracting precisely the blockage signature, which leads to unexpected false alarms and thus, degrades the positioning performance. To address this issue, we first empirically analyze the behavior of the sector detection error as a function of the corresponding SSIM percentile in the last column vector $\boldsymbol{m}_j[k]$ of the corresponding matrix $\boldsymbol{M}_j[k]$. Intuitively, a "good" detection shall result in a low percentile value. Let $f(m)$ be the empirical cumulative probability density function of $\boldsymbol{m}_j[k]$, we thus compute the indicator $f(\boldsymbol{m}_j[k]|_{s=\hat{s}[k]})$ corresponding to the detection decision $\hat{s}[k]$. On Fig. 3, the latter percentile is shown to be fairly correlated to the angular errors, with a steeper increase beyond 60% likely due to false alarms. Thus, it indirectly reveals when the blocker's power signature can be reliably exploited for RIS selection and/or weighting purposes, as follows:

a) Selection: One RIS contribution at time k is rejected if the instantaneous percentile value $f(\boldsymbol{m}_j[k]|_{s=\hat{s}[k]})$ exceeds a threshold, which is empirically set to 60% (See Fig. 3).

b) Weighting: The uncertainty $\alpha'_j[k]$ in (8) is determined based on the mean or maximum error functions of the instantaneous percentile value $f(\boldsymbol{m}_j[k]|_{s=\hat{s}[k]})$ (from Fig. 3).

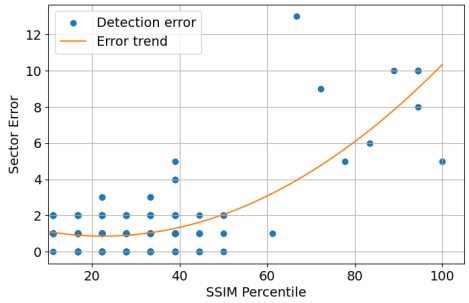

Fig. 3: Scatter plot of detected sectors' index errors (over all time instants), as a function of the SSIM percentile (along with its data-fitted quadratic interpolant).

IV. Numerical Analysis

A. Simulation Scenario and Parameters

We consider a network of $M = 24$ BSs and $N = 106$ UEs. The BSs are uniformly distributed on the edges of a rectangular area of $160\text{m} \times 80\text{m}$ and each BS is in communications with its 4 closest UEs, with tranmist power $P_{Tx} = 33$ dBm. A system of $J = 10$ 40×20-element dual-beam RISs is placed on 2 parallel horizontal lines, each 20m from the center of the network. An example of network deployment is shown in Fig 4. Without loss of generality, we assume DL communications at 28 GHz in a bandwidth of 400 MHz, so that all the transmitting BSs contribute as non-coherent sources to the ambient power received after reflection at the J sensing nodes, which are associated with their respective closest RISs. It is also supposed that the RISs scan all their sectors in a synchronous way between two consecutive detection events. We apply exacly the signal and channel propagation models as in [4], incl. the path loss model from [16], after averaging out the fast-fading but preserving all slow-fading contributions. Finally, we assume a default angular granularity of 10° for RIS beam scanning, leading to $S = 18$ angular sectors per RIS, and a time window of $\Delta = 30$ for building the scanning matrix. Finally, $R_B = 3$ m and $A = 100$ dB.

B. Simulation Results and Discussion

Fig 5 presents the detected sectors of some RISs with and without applying the rejection. As a result, most of false alarms are eliminated. However, some outliers, for instance in case of RIS 1, still pass the rejection test since the mean errors corresponding to their SSIM percentile are relatively small.

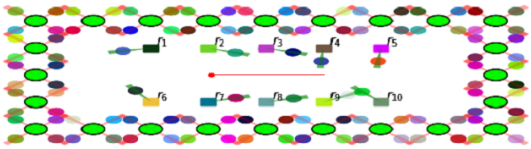

Fig. 4: Canonical network deployment considered in simulations (red straight line: blocker's trajectory, big circles: BSs, small circles: UEs (incl. sensing-nodes), rectangles: RISs).

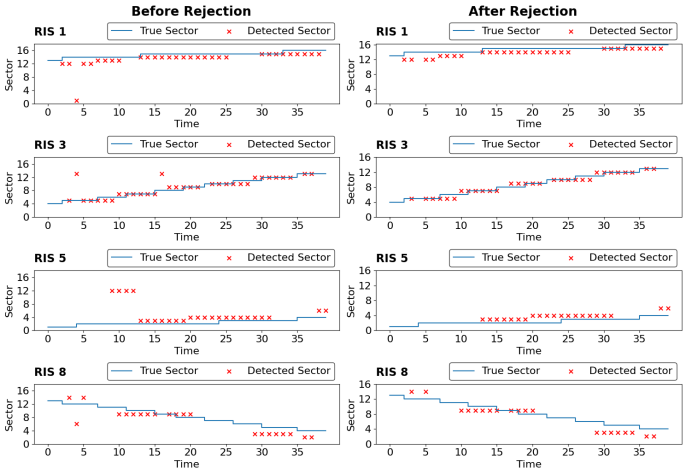

Fig. 5: Impact of SSIM-based rejection on false alarms while detecting occupied angular sectors (Ex. for 4 representative RISs).

Fig 6 shows the empirical CDF of localization error with various pre-processing strategies. We can then notice that regardless of the number of involved RISs, the errors exhibit approximately the same trends. Particularly, the Max weighting method after rejection is more accurate than the raw detection, leading typically to error gains of 3m and 5m at 68% and 95% of the CDF in case at least 5 RISs are used, respectively. It also outperforms the Mean weighting by considering the worst-case scenario. On another hand, when having 7 or more available RISs, the high CDF performance improves (in the large errors regime), as the uncertainty region decreases when the number of collaborative RISs increases. These results emphasize the importance of selective cooperation within such an opportunistic RIS-aided sensing scheme.

V. Conclusion

In this paper, we have presented a cooperative sensing approach relying on spatially distributed dual-beam RISs, which can opportunistically leverage the presence of ambient non-coherent radio sources in very dense mmWave networks to position a moving obstacle based on received power measurements. Simulations show that basic indicators inheriting from image processing, typically applied to the results of the SVD-based source seperation, contribute to both improve RIS-wise detection performances and properly select/weight RIS contributions for cooperative positioning. Future works will assess the sensitivity of the proposed technique to intermittent and/or mobile non-coherent sources, as well as to multiple

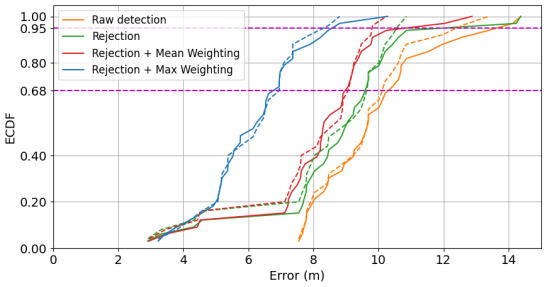

Fig. 6: Empirical CDF of blocker's estimated location error while using at least 5 (solid line) or 7 RISs (dashed line) in cooperative positioning, for various pre-processing strategies.

obstacles. We will also investigate resource allocation schemes enabling relevant communication-detection trade-offs.

Acknowledgement

This work was supported by the European Commission through the 6G-DISAC Project under the SNS HORIZON program (no. 101139130), as well as by the French National Research Agency (ANR-22-PEFT-0005), as part of France 2030 through the NF-YACARI project.

References

[1] M. Sana *et al.*, "Multi-Agent Deep Reinforcement Learning For Distributed Handover Management In Dense MmWave Networks," in *proc. IEEE ICASSP'20*, pp. 8976–8980, 2020.

[2] R. Hersyandika *et al.*, "Guard Beam: Protecting mmWave Communication through In-Band Early Blockage Prediction," in *proc. IEEE GLOBECOM'22*, pp. 4093–4098, 2022.

[3] T. Gu *et al.*, "Beamsniff: Enabling Seamless Communication under Mobility and Blockage in 60 GHz Networks," in *proc. IFIP NETWORKING'19*, 2019.

[4] M. Sana *et al.*, "Sensing of Side Lobes Interference for Blockage Prediction in Dense mmWave Networks," in *proc. IEEE PIMRC'23*, 2023.

[5] M. Schmidhammer *et al.*, "Multipath-Enhanced Device-Free Localization in Wideband Wireless Networks," *IEEE Ant. Wir. Propag. Letters*, vol. 20, no. 4, pp. 453–457, 2021.

[6] H. Dakdouk *et al.*, "Cooperative Sensing of Side Lobes Interference for mmWave Blockages Localization and Mapping," in *proc. Joint EuCNC'24 & 6G Summit'24*, 2024.

[7] M. Rupp *et al.*, "An LS Localisation Method for Massive MIMO Transmission Systems," in *proc. IEEE ICASSP'19*, pp. 4375–4379, 2019.

[8] Z. Ali *et al.*, "Early Warning of mmWave Signal Blockage and AoA Transition using sub-6 GHz Observations," *IEEE Com. Letters*, vol. 24, no. 1, pp. 207–211, 2019.

[9] C. Vaca-Rubio *et al.*, "Radio Sensing with Large Intelligent Surface for 6G," in *proc. IEEE ICASSP'23*, 2023.

[10] F. Devoti *et al.*, "PASID: Exploiting Indoor mmWave Deployments for Passive Intrusion Detection," in *proc. IEEE INFOCOM'20*, pp. 1479–1488, 2020.

[11] J. L. Gonzalez-Jimenez *et al.*, "A 58 Gb/s D-Band NLOS Communication System Enabled by Active RIS," in *proc. EuMW'25*, 2025. (to appear).

[12] T. Arshed *et al.*, "Surface-Wave Metaprism for Smart Surface Communications," *IEEE Trans. on Ant. and Propag.*, 2025.

[13] W. Zhou *et al.*, "Image Quality Assessment: from Error Visibility to Structural Similarity," *IEEE Trans. Imag. Proc.*, vol. 13, no. 4, pp. 600–612, 2004.

[14] X. Li *et al.*, "Tutorial: Complexity Analysis of Singular Value Decomposition and its Variants," *arXiv:1906.12085*, 2019.

[15] M.-J. Chen *et al.*, "Fast Strutural Similarity Index Algorithm," *Journal Real-Time Image Proc.*, vol. 6, no. 4, pp. 281–287, 2011.

[16] A. Mudonhi *et al.*, "mmWave Massive MIMO Channel Sounding in Industrial IoT Scenarios," in *proc. Joint EuCNC'22 & 6G Summit'22*, pp. 53–58, 2022.